

Role of Strain on the Coherent Properties of GaAs Excitons and Biexcitons

Brian L. Wilmer,¹ Daniel Webber,² Joseph M. Ashley,^{1,†} Kimberley C. Hall,² and Alan D. Bristow^{1,*}

¹*Department of Physics and Astronomy, West Virginia University, Morgantown, West Virginia 26506-6315 USA*

²*Department of Physics and Atmospheric Science, Dalhousie University, Halifax, Nova Scotia, B3H4R2 Canada*

Abstract: Polarization-dependent two-dimensional Fourier-transform spectroscopy (2DFTS) is performed on excitons in strained bulk GaAs layers probing the coherent response for differing amounts of strain. Biaxial tensile strain lifts the degeneracy of heavy-hole (HH) and light-hole (LH) valence states, leading to an observed splitting of the associated excitons at low temperature. Increasing the strain increases the magnitude of the HH/LH exciton peak splitting, induces an asymmetry in the off-diagonal coherences, increases the difference in the HH and LH exciton homogenous linewidths, and increases the inhomogeneous broadening of both exciton species. All results arise from strain-induced variations in the local electronic environment, which is not uniform along the growth direction of the thin layers. For cross-linear polarized excitation, wherein excitonic signals give way to biexcitonic signals, the high-strain sample shows evidence of bound LH, HH, and mixed biexcitons.

PACS: 78.40.Fy, 78.47.jh, 71.70.Fk, 77.80.bn

I. INTRODUCTION

Strain engineering provides a powerful method to tailor the electronic and optical properties of semiconductors, a feature that has been utilized in a variety of applications in semiconductor optoelectronics. For instance, the controlled use of strain has led to low-threshold lasers using strained quantum wells or quantum dot systems,¹⁻⁴ and fast field-effect transistors based on the SiGe/Si system.⁵ Manipulation of strain may also lead to the development of polarization-entangled photon pairs through control of the relative size of the exciton and biexciton binding energies in quantum dot systems,⁶ and provides a means to dynamically manipulate the spin-orbit interaction for possible spin-sensitive electronic devices.^{7,8} For such applications, an accurate characterization of the influence of strain on the local and global optoelectronic properties in the semiconductor heterostructure is essential. Existing studies of strain in semiconductor systems have largely focused on its influence on the energetic locations of the heavy-hole and light-hole exciton resonances, detected using optical techniques such as photoluminescence, reflectivity and Raman scattering.⁹⁻¹⁵ The exciton peak positions may be understood taking into account the hydrostatic and uniaxial stress components, the latter of which lifts the degeneracy in the valence bands.¹¹

Coherent nonlinear optical techniques, such as two-dimensional Fourier-transform spectroscopy (2DFTS), provide a more comprehensive picture of the excitonic response compared to linear optical techniques. 2DFTS may be exploited to gain further insight into the influence of strain on the coherent optical response of semiconductors. For instance, the ability to independently measure the levels of homogeneous and inhomogeneous broadening¹⁶⁻²¹ may yield insight into varying local electronic environments tied to partial strain relaxation in thin film systems. 2DFTS has also provided a wealth of information about many-body interactions (MBI) in quantum well systems through the ability to isolate a range of quantum pathways from the excitons, their coupling to one another, and biexcitons.²²⁻³² The study of such effects in a bulk semiconductor system, in which the splitting between the exciton resonances is caused exclusively by strain, would provide insight into the influence of strain on MBI and the coherent response of the excitons.³³

In this paper, 2DFTS is used to study bulk excitons in two GaAs layers with different thicknesses, such that the two samples exhibit different amounts of strain resulting from being attached to sapphire disks and cooled. Comparison of rephasing 2DFTS spectra with collinear and cross-linear polarization configurations allows for the observation of the line shapes, center positions, homogeneous and inhomogeneous linewidths, and the coupling of light- (LH) and heavy-hole (HH) excitons and biexcitons. In addition to increasing the separation between the HH and LH excitons, these experiments show that

increasing the amount of strain in the bulk semiconductor modifies the relative strengths of the off-diagonal exciton features, altering the spectrum from a coherent response seen in atomic vapors to one seen in quantum wells. A larger degree of inhomogeneous broadening is also observed in the sample with larger strain, attributed to variations in the local electronic environment that are likely tied to strain gradients along the growth direction of the heterostructure. Significant bound biexcitons signatures are visible for cross-linear polarized excitation, due to the presence of few-body interactions. Overall, the results suggest that 2DFTS and the coherent response of GaAs excitons is highly sensitive to strain.

II. EXPERIMENTAL

Samples of intrinsic GaAs are grown by molecular-beam epitaxy to have thicknesses of 300 nm and 800 nm along with etch stop layers. The samples are glued to sapphire disks and the GaAs substrates are removed for optical transmission measurements. All measurements were performed at 10 K in a cold finger cryostat. Cooling leads to uniform contraction of the sapphire and the different coefficients of thermal expansion for GaAs and sapphire results in two-dimensional in-plane tensile strain of the thin GaAs layers.³⁴ This in-plane strain necessarily causes slight compressive strain along the growth direction, in an attempt to maintain the GaAs unit cell volume. Strain is able to relax along the growth direction away from the point of attachment to the sapphire. The two samples possess different effective strain values, as well as differing variations in the local electronic environment due to differing amounts of strain relaxation along the growth direction.

Absorption and 2DFTS measurements were performed with resonant excitation. The 2DFTS setup, shown in Fig. 1, is described fully in previous work.^{35,36} In brief, a mode-locked Ti:sapphire laser oscillator generates ~ 100 fs pulses at a repetition rate of 76 MHz. The pulses are split into four equal strength replicas, attenuated to an average power of 0.2 mW per beam and arranged on four corners of a box. Pulses A^* , B , and C excite the sample and can be independently adjusted to control the delay times τ and T (see inset of Fig. 1 for time sequence), while maintaining a phase stabilization of $< \lambda/100$. The three excitation pulses impinge the sample at non-normal incidence allowing for spatial selection of the emitted transient TFWM signal emitted in the background-free $\mathbf{k}_{\text{Sig}} = -\mathbf{k}_A + \mathbf{k}_B + \mathbf{k}_C$ phase-matching direction. This phase-matching condition selects the rephrasing spectrum with the pulse ordering A^* , B , C , where the star denotes the phase-conjugated pulse.

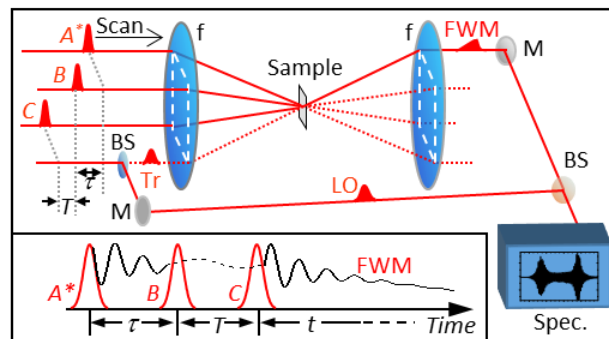


Fig. 1 (Color online) Experimental setup for the multidimensional coherent spectroscopy with the sample at the focus. (f = lens, M = mirror, BS = beam splitter, FWM = four-wave-mixing signal, τ = period between pulses A^* and B , T = period between pulses B and C , and t = period after pulse C triggers the emission, Tr = tracer beam, traces the phase-matched direction, LO = local oscillator for spectral interferometry, and $Spec$ is the imaging spectrometer with CCD). The inset shows the rephrasing excitation pulse sequence.

The emitted signal is collected in a spectrometer with a cooled CCD camera following detection of the local oscillator (LO) pulse, which is routed around the sample to avoid unwanted pre-excitation or reference distortions. A time delay of several picosecond between the LO and signal produces spectral interference fringes that allow the complex spectrum to be extracted. Spectral interferograms are collected

as a function of delay time τ , which is stepped in precise, phase-controlled increments to generate a series of measurements of delay time versus the emission photon energy.

A two-dimensional spectrum is acquired by performing a numerical Fourier transform with respect to the delay time τ . For rephasing spectra, the transform results in the absorption photon energy being negative and the diagonal of the spectrum is chosen to point down and to the right. For all spectra shown in this work, the mixing delay time T is set to 100 fs to enforce strict time ordering and all excitation and emission pulses are set with either collinear (XXXX) or cross-linear (XYYX) polarization configurations (where the first three terms indicate the excitation and the fourth term indicates the emission polarization states).²⁴ Excitation irradiances are limited to ensure the response is in the $\chi^{(3)}$ nonlinear optical regime and the laser pulses are centered over the midpoint between the HH and LH excitations observed in the linear spectra.

III. RESULTS AND DISCUSSION

Figure 2(a) shows the linear absorption of the 300-nm (red) and 800-nm (blue) GaAs layers. The spectra show sharp resonances due to the LH and HH excitons with increasing energy and the electron-hole continuum at even higher energies. Degeneracy lifting and biaxial tensile strain puts the LH band energetically higher than the HH band as evidenced by the narrow LH peak position relative to the HH position. The thinner and thicker sample has a splitting between the exciton resonances of ~ 6 and ~ 3 meV, respectively. It is known that strain, among other variables, alters the band structure. Perturbative strain linearly shifts the bands by an amount given by $E_{shift} = \mathcal{E}(\Delta a/a)$, where \mathcal{E} is the deformation potential, a is the lattice constant, and Δa is the change in lattice constant due to stress.³⁷ Uniform biaxial in-plane strain lifts the degeneracy of the HH and LH valence bands, given by $\Delta E = 2|b|\Delta e$,^{38,39} where b is the shear deformation potential, and $\Delta e = e_{xx} - e_{zz}$ is the effective strain difference between the in-plane and out-of-plane directions. Using the literature value $b = -1750$ meV,⁴⁰ effective strain differences of $0.18 \pm 0.02\%$ and $0.08 \pm 0.02\%$ are determined for the thinner and thicker GaAs layers respectively; see Fig. 2(b). In the figure, the error bars are smaller than the size of the data markers.

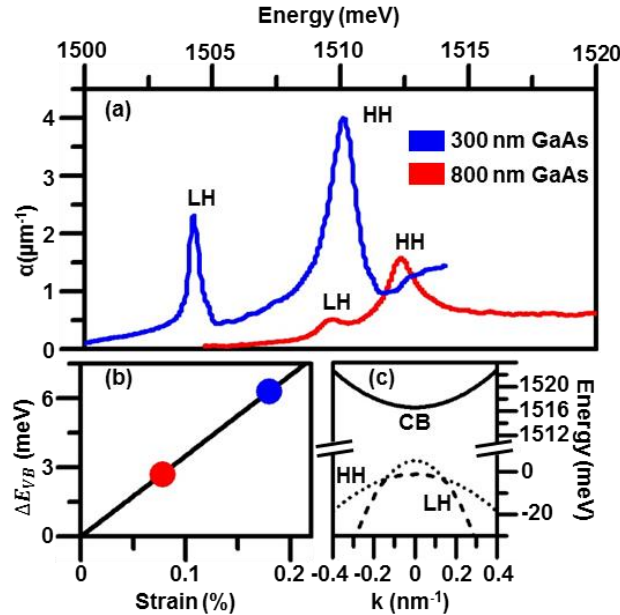


Fig. 2 (color online) (a) Linear optical absorption spectra for a 300-nm (high strain) and 800-nm (low strain) GaAs layers revealing strain-split heavy- (HH) and light-hole (LH) excitons. (b) Effective strain (Δe) versus the exciton splitting (ΔE) for both samples. (c) Single-particle dispersions of the conduction, HH and LH valence bands.

Previously published $k \cdot p$ models,⁴¹ result in quadratic dispersions for the conduction E_{cb} , HH E_H and LH E_L valence bands. The dispersions are modified by linear shifts terms at the Γ -point and band

mixing away from $k = 0$, which affects both the quadratic term and adds a third term. Final equations within an effective 1D model are simplified by assuming $e_{xx} = e_{yy}$, giving:

$$E_{cb} = \frac{\hbar^2}{2m_c}k^2 + E_g + a_c(2e_{xx} + e_{zz}), \quad (1)$$

$$E_L = -\frac{\hbar^2}{2m_e}\gamma_1k^2 + a_v(2e_{xx} + e_{zz}) + \left| \frac{\hbar^2}{2m_L}\gamma_2k^2 - b(e_{xx} - e_{zz}) \right|, \quad (2)$$

and

$$E_H = -\frac{\hbar^2}{2m_e}\gamma_1k^2 + a_v(2e_{xx} + e_{zz}) - \left| \frac{\hbar^2}{2m_H}\gamma_2k^2 - b(e_{xx} - e_{zz}) \right|. \quad (3)$$

The literature values for the effective masses of the conduction band, LH band, and HH band electrons are, $m_c = .066m_e$, $m_L = .094m_e$, and $m_H = .34m_e$ ⁴² (where m_e is the elementary electron mass), the low temperature, unstrained band gap is $E_g = 1518.9$ meV,⁴³ the valence band deformation potential is $a_v = 1600$ meV, the conduction band deformation potential is $a_c = -7000$ meV and the Luttinger parameters are $\gamma_1 = 6.98$, and $\gamma_2 = 2.06$.³ The band gap is ~ 1512.8 meV, determined from the onset of the electron-LH continuum in Fig. 2(a). Using this in conjunction with observed valence band splitting, fitting parameters e_{xx} and e_{zz} yield strains of 0.07% and -0.11% in the xy plane and z directions respectively for the high-strain sample. This gives the band edges of 1516.6 meV, 4.7 meV, and -1.5 meV for the conduction, LH valence and HH valence bands respectively. Using these values, equations (1)-(3) are plotted in Fig. 2(e). Away from the band Γ point, anti-crossings appear where the HH and LH band are in close proximity, although this is out of the accessible range of wave vectors used in the experiment. Within the light cone near the Γ point $E_L > E_H$, such that the lower energy spectral feature is the LH exciton. Similar analysis can be performed for the low-strain sample.

The third-order response of the excitonic system can be described by double-sided Feynman diagrams that traverse the available levels for the quantum system.²⁶ Figure 3(a) shows the level diagram arising from a Hilbert space transform of the electronic states in bulk GaAs including the spin degeneracy and strain splitting. Optical transitions are shown in the circular basis, where σ^- and σ^+ correspond to left and right circular polarization. The resulting transitions are a ground state $|g\rangle$ indicating no optical excitation, HH and LH excitons, denoted $|h\rangle$ and $|l\rangle$ respectively, and four biexcitons, denoted $|hh\rangle$, $|ll\rangle$, $|hl\rangle$ and $|lh\rangle$. Note that the spin quantum number has been omitted for ease of discussion of linearly polarized excitation.

Quantum pathways traversing the level diagram obey time-ordering and phase-matching condition corresponding to the rephrasing $-\mathbf{k}_A + \mathbf{k}_B + \mathbf{k}_C$. Signals must occur from excitation by all three pulses; hence, the language of polarization and population can be employed as a result of successive interactions with odd and even numbers of laser pulses. The first pulse drives a polarization between the ground and an excited state, the second pulse leads to a population (or an excited-state coherence) and the third pulse drives a polarization that radiates as the FWM signal. Panel (b) shows ground-state bleaching (GSB) pathways, where the second pulse creates a population in the ground state. Panels (c) shows excited-state emission (ESE) pathways, where the second pulse drives a population/polarization in the first excited states (excitonic) manifold. In 2DFTS spectra both GSB and ESE pathways result in diagonal intra-action features for both exciton species and two off-diagonal interaction features that are a result of coupling between the two exciton species. Panel (d) shows excited-state absorption (ESA) pathways, where the signal arises from a final population of the excited state and includes a polarization between the excitonic and second-excited (biexcitonic) manifolds. In 2DFTS spectra this can be used to identify the bound biexciton contributions, because the biexciton binding energy results in a shift in the emission energy relative to the absorption energy. To date 2DFTS has revealed biexcitons features adjacent to the heavy-hole exciton in GaAs

quantum wells,^{23,24} interfacial quantum dot distributions⁴⁵ and upper branch exciton-polaritons in semiconductor microcavities.⁴⁶

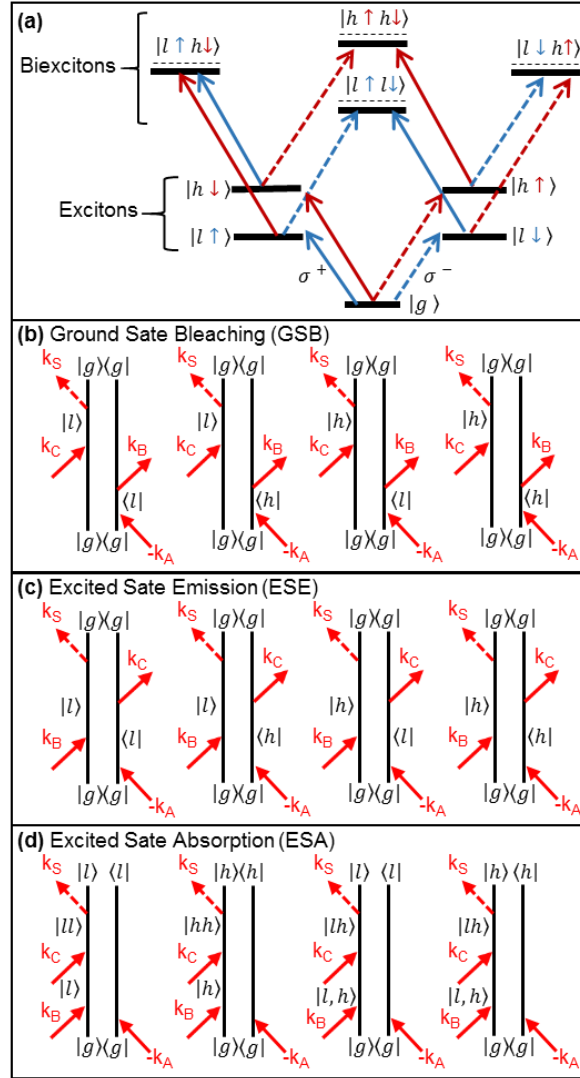


Fig. 3 (color online) (a) Exciton level diagram for strain-split bulk excitons and biexcitons in GaAs. Double-sided Feynman diagrams illustrate the quantum pathways of (b) ground state bleaching, (c) excited state emission and (d) excited state absorption.

Figure 4 shows the 2DFTS rephasing spectra for low- (0.08%) and high-strain (0.18%) samples: (a) amplitude and (e) real parts of the XXXX polarized spectra are shown for the low-strain sample; (b) and (f) show the same for XYYX polarization. Similarly, high-strain spectra are shown in panels (c), (d), (g) and (h). All spectra are normalized to their strongest feature. First, it is worth discussing the spectral features that are common to both samples. Each spectrum is dominated by four star-like features as described above, namely two diagonal (X_L and X_H) and two off-diagonal (X_L - X_H and X_H - X_L) coherences. In addition, XXXX polarized spectra for both samples show two vertical streaks (denoted C_L and C_H), which are coherences resulting from MBI between the electron-hole continuum and the X_L and X_H resonances.^{33,47} Selecting XYYX polarization is known to suppress MBI,^{48,49} such that in 2DFTS spectra the signals are reduced by a factor of approximately five, the C_L and C_H features are strongly reduced, the off-diagonal features become similar or weaker than the diagonal features,^{23,24} and biexciton features become more prominent.^{24,45} The latter effect is more pronounced for the high strain sample. For both samples, dispersive

line shapes are observed in the real part of the XXXX polarized spectra as a result of the MBI.^{22,23} For XYYX polarization, with suppressed MBI, the spectral features become peaked about their center position. For the case of the diagonal features, this means they are centered on the diagonal with positive sign, while off-diagonal features are centered at positions corresponding to absorption into one exciton species and emission from the other with negative sign.

Increasing the strain from 0.08% to 0.18% has several effects on the coherent properties observed in the 2DFTS rephrasing spectra. As seen in the linear spectra, the splitting between the two exciton resonances increases with strain. The spectral coordinates $\{E_{\text{abs}}, E_{\text{emi}}\}$ of the four main features X_L , X_H , X_L-X_H and X_H-X_L are listed in Table 1 for both low- and high-strain samples. The increased splitting has the effect of making the exciton species more energetically distinct and there is a change in spectral weights of the four main features in Fig. 4(a) and (c). It can be seen that in the low-strain sample the X_H has larger oscillator strength than X_L , and that X_L-X_H and X_H-X_L are equal in magnitude, with strengths that are approximately the average of X_L and X_H . This result is reminiscent of the coherent response of three-level atomic vapors,⁵⁰ indicating a symmetric coupling between the two exciton species.²⁶ On the other hand, in the high-strain sample the lower energy exciton X_L is stronger than X_H and the relative strengths of the off-diagonal become asymmetric, with X_L-X_H increasing by approximately the same amount that X_H-X_L decreases. This asymmetry is a signature of the excitation-induced dephasing (EID) and EIS.^{22,47} This is reminiscent of the coherent response lower dimensional GaAs systems, where the $T = 100$ fs to prevent incoherent relaxation. The comparison of the two results suggest a greater impact of MBI in the high-strain sample. More study is required to elucidate the role of MBI in the two samples.³³

Table 1 Spectral coordinates for the exciton and biexciton features in units of meV and with error of ~ 0.1 meV. Exciton and biexciton features are extracted from XXXX and XYYX spectra respectively.

<u>Spectral Feature</u>	<u>Low Strain</u> (0.08%)		<u>High Strain</u> (0.18%)	
	E_{abs}	E_{emi}	E_{abs}	E_{emi}
X_L	-1509.7	1509.7	-1503.5	1503.5
X_H	-1512.4	1512.4	-1510	1510
X_L-X_H	-1512.4	1509.7	1510	1503.5
X_H-X_L	-1509.7	1512.4	-1503.5	1510
B_H	-	-	-1510.2	1508.2
B_L	-	-	-1503.8	1502.8
B_M	-	-	-1503.8	1509

Another prominent effect of the increased strain is the presence of new features in XYYX rephrasing spectra, which tend to be more sensitive to bound biexciton contributions that arise from ESA pathways; see Fig. 3(d). The real-part of XYYX spectrum [Fig. 4(h)] exhibits a strong negative B_H feature. Spectral coordinates $\{E_{\text{abs}}, E_{\text{emi}}\}$ are listed in Table 1 revealing the shift in the emission energy that corresponds to the biexciton binding energy. This contributions arises from the ESA pathway shown second to left in Fig. 3(d) and has been observed in other excitonic systems as discussed above. In addition, new features are observed at B_L , which is associated with a LH biexciton and the most left double-sided Feynman diagram in Fig. 3(d), and at B_M , which is associated with a mixed biexciton and the right most double-sided Feynman diagram of the same series. Energetically, the mixed biexciton pathway involves pulse A creating a polarization between $|g\rangle$ and $|h\rangle$, pulse B creating a polarization in either $|h\rangle$ or $|l\rangle$, pulse C creating a polarization with $|lh\rangle$ or $|hl\rangle$ and the emission releasing a photon with energy $E_H - \Delta E_M$ and returning the system to a population in $|h\rangle$. From the lateral shifts of the three biexcitonic features determined from the spectral coordinates listed in Table 1, it is estimated that the binding energies are ~ 1 meV and ~ 2 meV for the LH and HH biexcitons, which compare well to literature values.⁴⁴ Averaging the two pure biexciton

binding energies gives a value close to observed mixed biexciton binding energy, $\Delta E_M = 1.2 \pm 0.2$ meV. The presence of the mixed biexciton enhances the X_H - X_L feature in the normalized amplitude spectra for this polarization [Fig. 4(d)], as compared to the EID and EIS enhancement of the X_L - X_H feature for XXXX polarization [Fig. 4(c)]. To the best of the authors knowledge, mixed biexcitons have been theoretically explored in one-quantum (rephrasing)²⁶ and two-quantum⁵¹ 2DFTS and experimentally observed in two-quantum spectra,²⁵ but have not been directly observed in rephrasing spectra. Biexciton contributions are not observed in the low-strain sample, likely because of the relatively small HH/LH splitting compared to the biexciton binding energy.

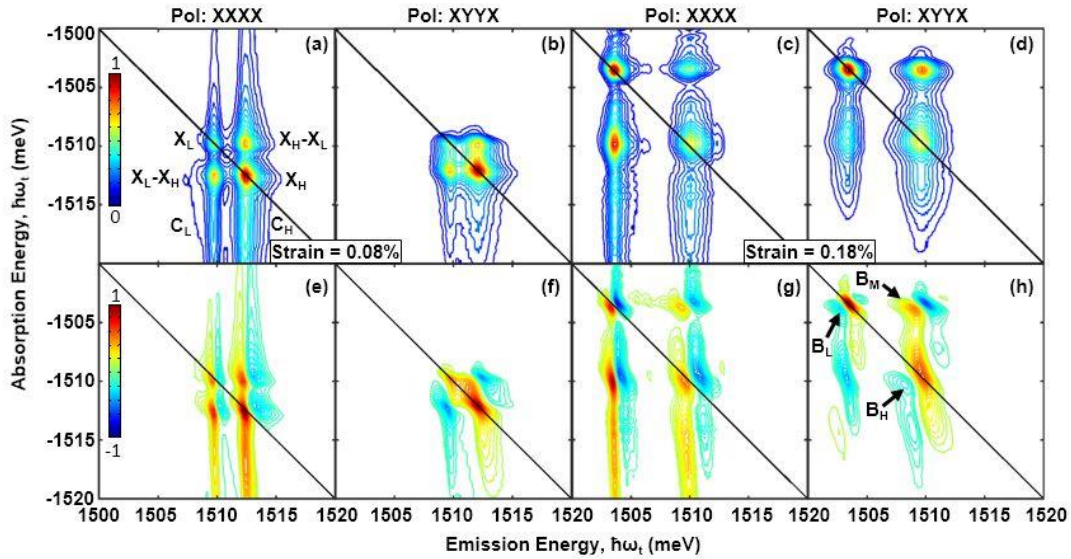


Fig. 4 (color online) Rephasing 2DFTS spectra for XXXX and YYYY polarization of the low-strain (0.08%) and high-strain (0.18%) GaAs samples. Panels (a)-(d) show the normalized amplitude and panels (e)-(h) show the corresponding real part of the spectra. Diagonal (intra-action) coherence X_L and X_H are the LH and HH excitons respectively, off-diagonal (interaction) coherences X_L - X_H and X_H - X_L reveal coupling between exciton species. Features C_L and C_H are electron-hole continuum coherences with their respective excitons. Features B_L , B_H , and B_M correspond to LH, HH, and mixed biexciton coherences.

Star-like line shapes indicate that the exciton coherences have negligible inhomogeneous broadening,¹⁸ as might be expected for bulk excitons where the excitonic Bohr radius is more than an order of magnitude smaller than the GaAs layer thickness. This contrasts with 2DFTS spectra for excitons in low-dimensional semiconductors, where local variations in quantum confinement within the excitation spot lead to significant inhomogeneous broadening and spectral features that are elongated along the diagonal direction. Nonetheless, the degree of inhomogeneous broadening is acquired using the analysis method of Siemens *et al.*¹⁸ which simultaneously fits the diagonal and cross-diagonal slices of each spectral feature, relating the line shapes to the homogeneous (Γ) and inhomogeneous (σ) linewidths.

Table 2 shows the extracted linewidths from the X_L and X_H diagonal features for the four amplitude spectra shown in Fig. 4(a) to (d). The error associated with each value from averaging is approximately 10% or 0.07 meV. The presence of the biexcitons complicates the YYYY spectra and direct comparison between polarizations. Nonetheless, comparisons can be made for the two samples for the same polarization. Both excitons for all spectra show $\Gamma \geq \sigma$ within the experimental uncertainty, indicating that the features are indeed all primarily homogeneously broadened. Moreover, the homogeneous linewidths of X_L is smaller than for X_H when excited by XXXX polarization, where excitonic linewidths are more accurate. This result is consistent with visual inspection of both linear and 2DFTS measurements. For both polarizations, the homogeneous linewidths of X_L and X_H are more comparable in the low-strain sample than the high-strain sample, consistent with the change in coupling discussed above. Namely, closer spaced

energy levels leads to comparable line shapes, as well as comparable amplitudes of the off-diagonal elements. Similar changes in the distinguishability of 2DFTS features has been observed in wedged semiconductor microcavities,⁴⁶ where the energy separation between lower and upper branches of the exciton-polaritons can be tuned to vary the interactions strength.

Table 2 Homogeneous (Γ) and inhomogeneous (σ) linewidths, with units of meV and an error of $\sim 10\%$.

	<u>Strained</u> <u>excitons</u>	<u>XXXX</u>		<u>YYYY</u>	
		Γ	σ	Γ	σ
0.08%	X _L	0.44	0.06	0.74	0.21
	X _H	0.46	0.27	0.59	0.33
0.18%	X _L	0.29	0.34	0.29	0.27
	X _H	0.70	0.41	0.87	0.31

Turning attention to the inhomogeneous broadening, it can be seen that in all cases σ is larger for X_H than for X_L, as has been observed in quantum wells.¹⁹ The inhomogeneous broadening is also larger in the high-strain sample. This indicates a larger degree of variation in the microscopic electronic environment within the excitation volume. Since no variation is expected in the plane of the sample, these variations are attributed to strain relaxation in the growth direction. Assuming this is the inhomogeneous broadening mechanism, then the relative change in effective strain across the sample depth, $\delta[\Delta e(z)]$, can be determined from the extremes of the exciton separation due to the calculated inhomogeneous broadening parameters extracted in Table 2. For example, at one extreme the inhomogeneous broadening red shifts the X_L from the average line center, while blue shifting the X_H from the average line center, such that $(E_H + \sigma_H/2) - (E_L + \sigma_L/2)$. The other extreme is for the opposite red and blue shift, such that $(E_H - \sigma_H/2) - (E_L - \sigma_L/2)$. To find the total change in strain we subtract the two cases and divide by two to avoid double counting. The change in strain is equivalent to the average of the two inhomogeneous linewidths. Employing the same conversion used for the average line centers in Fig. 2(b), the change in the effective strain is $[\Delta e(z)] = (\sigma_H + \sigma_L)/4|b|$. The inhomogeneous shifts are 0.69 meV and 1.31 meV for the low- and high-strain samples respectively, which corresponds to a variation in relative strain of 0.020% and 0.037% for the two samples. If it is also assumed that the strain relaxation is uniform over the thickness then the effective strain relaxation length for the two samples is $\sim 246 \text{ cm}^{-1}$ for the 800 nm thick sample and $1,247 \text{ cm}^{-1}$ for the 300 nm thick sample. These numbers reflect the situation that the thinner sample has a steeper strain relaxation gradient and larger overall inhomogeneous broadening contribution.

IV. CONCLUSIONS

Two samples of bulk GaAs attached to sapphire discs experience differing amounts of biaxial tensile strain due to their relaxation over differing volumes upon cooling. Strain splits and shifts the observed HH and LH excitons in optical absorption and 2DFTS, which is used to measure the coherent response. Increasing the strain has several effects on the exciton resonances: (i) the separation between the excitons increases; (ii) the strength of off-diagonal coherences become more asymmetric; (iii) the difference between the HH and LH homogenous linewidths increases as a result of great energy separation; and (iv) the inhomogeneous broadening increases due to increases in the strain relaxation gradient in the growth direction for thinner samples.

By focusing on bulk films that are significantly thick compared to the excitonic Bohr radius, the influence of strain on the exciton and biexciton resonances is probed in the absence of quantum confinement observed in lower-dimensional systems. The application of 2DFTS extracts both the average strain level and strain gradients experienced by the exciton resonances. Using collinear polarization, the one-quantum excitonic features are enhanced by many-body interactions and dominate the spectra. The spectral weight of the excitons become sensitive to the degree of separation induced by the strain. For small HH/LH separation, the spectral weight of the 2DFTS features is more akin to an atomic vapor than the usual

semiconductor nanostructure response. Alternatively, increasing strain allows the spectra to begin exhibiting the effects associated with increased excitation-induced MBI.

It is also shown that biexcitons are more easily observed in structures with large average strain due to the large HH/LH splitting relative to the biexciton binding energy. For cross-linear polarization, no population grating is created and, as a result, signals contributions associated with MBI are suppressed, allowing biexciton contributions to be revealed. Biexcitons are a manifestation of few-body interactions and are also expected to be more prevalent in samples where the HH and LH states are distinct. In addition, the first evidence of a mixed biexciton observed by one-quantum 2DFTS is presented.

Overall, these results show the sensitivity of 2DFTS to strain through interrogation of the coherent response and effects on the spectral line shape and spectral weight of all visible features. In particular, the analysis of the inhomogeneous broadening of bulk excitons reveals strain gradients that are stronger in thinner GaAs layers. This significant change in the coherent response invites studies where the strain can be controlled and EID and EIS can be measured.³³ Information learned here is part of the growing series of studies aimed at using sophisticated optical spectroscopy to unravel the electronic environment inside micro and nanostructures.

ACKNOWLEDGEMENTS

We thank Richard P. Mirin, Margaret Dobrowolska, Xinyu Liu, and Jacek K. Furdyna for growing of the GaAs samples. Work at West Virginia University was funded by the West Virginia Higher Education Policy Commission (HEPC.dsr.12.29) and the National Science Foundation (CBET-1233795). Work at Dalhousie University was funded by Natural Sciences and Engineering Research Council of Canada. JMA was supported by the National Science Foundation through the Research Experience for Undergraduates program (DMR-1262075).

* E-mail: alan.bristow@mail.wvu.edu

† Current address: Department of Physics, Radford University, Radford, Virginia, 24142 USA

¹ B. Zhao, T.R. Chen, L.E. Eng, Y.H. Zhuang, A. Shakouri, and A. Yariv, *Appl. Phys. Lett.* **65**, 1805 (1994).

² D. Leonard, M. Krishnamurthy, C.M. Reaves, S.P. Denbaars, and P.M. Petroff, *Appl. Phys. Lett.* **63**, 3203 (1993).

³ A.-L. Barabási, *Appl. Phys. Lett.* **70**, 2565 (1997).

⁴ D.L. Huffaker, G. Park, Z. Zou, O.B. Shchekin, and D.G. Deppe, *IEEE J. Sel. Top. Quantum Electron.* **6**, 452 (2000).

⁵ T.E. Whall and E.H.C. Parker, *J. Phys. Appl. Phys.* **31**, 1397 (1998).

⁶ F. Ding, R. Singh, J.D. Plumhof, T. Zander, V. Křápek, Y.H. Chen, M. Benyoucef, V. Zwiller, K. Dörr, G. Bester, A. Rastelli, and O.G. Schmidt, *Phys. Rev. Lett.* **104**, 067405 (2010).

⁷ V. Sih, H. Knotz, J. Stephens, V.R. Horowitz, A.C. Gossard, and D.D. Awschalom, *Phys. Rev. B* **73**, 241316 (2006).

⁸ H. Knotz, A.W. Holleitner, J. Stephens, R.C. Myers, and D.D. Awschalom, *Appl. Phys. Lett.* **88**, 241918 (2006).

⁹ Y. Zhang, B.J. Skromme, and F.S. Turco-Sandroff, *Phys. Rev. B* **46**, 3872 (1992).

¹⁰ K.J. Moore, G. Duggan, K. Woodbridge, and C. Roberts, *Phys. Rev. B* **41**, 1090 (1990).

¹¹ K.S. Kim, G.M. Yang, H.W. Shim, K.Y. Lim, E.-K. Suh, and H.J. Lee, *J. Appl. Phys.* **82**, 5103 (1997).

¹² K.S. Kim, G.M. Yang, and H.J. Lee, *J. Vac. Sci. Technol. A* **16**, 2663 (1998).

¹³ C.M.N. Mateo, A.T. Garcia, F.R.M. Ramos, K.I. Manibog, and A.A. Salvador, *J. Appl. Phys.* **101**, 073519 (2007).

¹⁴ C.M.N. Mateo, J.J. Ibañez, J.G. Fernando, J.C. Garcia, K. Omambac, R.B. Jaculbia, M. Defensor, and A.A. Salvador, *J. Appl. Phys.* **104**, 103537 (2008).

¹⁵ B. Fluegel, A.V. Mialitsin, D.A. Beaton, J.L. Reno, and A. Mascarenhas, *Nat. Commun.* **6**, 7136 (2015).

¹⁶ I. Kuznetsova, T. Meier, S.T. Cundiff, and P. Thomas, *Phys Rev B* **76**, 153301 (2007).

¹⁷ I. Kuznetsova, N. Gógh, J. Förstner, T. Meier, S.T. Cundiff, I. Varga, and P. Thomas, *Phys. Rev. B* **81**, 075307 (2010).

¹⁸ M.E. Siemens, G. Moody, H. Li, A.D. Bristow, and S.T. Cundiff, *Opt. Express* **18**, 17699 (2010).

¹⁹ A.D. Bristow, T. Zhang, M.E. Siemens, S.T. Cundiff, and R.P. Mirin, *J. Phys. Chem. B* **115**, 5365 (2011).

²⁰ G. Moody, M. Siemens, A. Bristow, X. Dai, D. Karaiskaj, A. Bracker, D. Gammon, and S. Cundiff, *Phys. Rev. B* **83**, 115324 (2011).

- ²¹ Y.D. Glinka, Z. Sun, M. Erementchouk, M.N. Leuenberger, A.D. Bristow, S.T. Cundiff, A.S. Bracker, and X. Li, *Phys. Rev. B* **88**, (2013).
- ²² X.Q. Li, T.H. Zhang, C.N. Borca, and S.T. Cundiff, *Phys Rev Lett* **96**, (2006).
- ²³ T. Zhang, I. Kuznetsova, T. Meier, X. Li, R.P. Mirin, P. Thomas, and S.T. Cundiff, *Proc Nat Acad Sci* **104**, 14227 (2007).
- ²⁴ A.D. Bristow, D. Karauskaj, X. Dai, R.P. Mirin, and S.T. Cundiff, *Phys. Rev. B* **79**, (2009).
- ²⁵ D. Karauskaj, A.D. Bristow, L. Yang, X. Dai, R.P. Mirin, S. Mukamel, and S.T. Cundiff, *Phys. Rev. Lett.* **104**, 117401 (2010).
- ²⁶ L. Yang, I.V. Schweigert, S.T. Cundiff, and S. Mukamel, *Phys. Rev. B* **75**, 125302 (2007).
- ²⁷ L. Yang and S. Mukamel, *Phys Rev Lett* **100**, 057402 (2008).
- ²⁸ L. Yang, T. Zhang, A.D. Bristow, S.T. Cundiff, and S. Mukamel, *J. Chem. Phys.* **129**, 234711 (2008).
- ²⁹ D. Turner, K. Stone, K. Gundogdu, and K. Nelson, *J. Chem. Phys.* **131**, (2009).
- ³⁰ J. Kasprzak, B. Patton, V. Savona, and W. Langbein, *Nat. Photonics* **5**, 57 (2011).
- ³¹ C.R. Hall, J.O. Tollerud, H.M. Quiney, and J.A. Davis, *New J. Phys.* **15**, 045028 (2013).
- ³² G. Nardin, G. Moody, R. Singh, T.M. Autry, H. Li, F. Morier-Genoud, and S.T. Cundiff, *Phys. Rev. Lett.* **112**, 046402 (2014).
- ³³ D. Webber, B.L. Wilmer, X. Lui, M. Dobrowolska, J.K. Furdyna, A.D. Bristow, and K.C. Hall, *Prep.* (n.d.).
- ³⁴ T.P. Humphreys, J.B. Posthill, K. Das, C.A. Sukow, R.J. Nemanichi, N.R. Parikh, and A. Majeed, *Jpn. J. Appl. Phys.* **28**, L1595 (1989).
- ³⁵ A.D. Bristow, D. Karauskaj, X. Dai, T. Zhang, C. Carlsson, K.R. Hagen, R. Jimenez, and S.T. Cundiff, *Rev. Sci. Instrum.* **80**, 073108 (2009).
- ³⁶ A.D. Bristow, D. Karauskaj, X. Dai, and S.T. Cundiff, *Opt. Express* **16**, 18017 (2008).
- ³⁷ C.F. Klingshirn, *Semiconductor Optics* (Springer Berlin Heidelberg, Berlin, Heidelberg, 2012).
- ³⁸ C.M.N. Mateo, A.T. Garcia, F.R.M. Ramos, K.I. Manibog, and A.A. Salvador, *J. Appl. Phys.* **101**, 073519 (2007).
- ³⁹ C.M.N. Mateo, J.J. Ibañez, J.G. Fernando, J.C. Garcia, K. Omambac, R.B. Jaculbia, M. Defensor, and A.A. Salvador, *J. Appl. Phys.* **104**, 103537 (2008).
- ⁴⁰ A. Gavini and M. Cardona, *Phys. Rev. B* **1**, 672 (1970).
- ⁴¹ Y. Sun, S.E. Thompson, and T. Nishida, *J. Appl. Phys.* **101**, 104503 (2007).
- ⁴² S.T. Cundiff, *Opt. Express* **16**, 4639 (2008).
- ⁴³ E. Grilli, M. Guzzi, R. Zamboni, and L. Pavesi, *Phys. Rev. B* **45**, 1638 (1992).
- ⁴⁴ I. Vurgaftman, J.R. Meyer, and L.R. Ram-Mohan, *J. Appl. Phys.* **89**, 5815 (2001).
- ⁴⁵ G. Moody, R. Singh, H. Li, I.A. Akimov, M. Bayer, D. Reuter, A.D. Wieck, A.S. Bracker, D. Gammon, and S.T. Cundiff, *Phys. Status Solidi B* **250**, 1753 (2013).
- ⁴⁶ B.L. Wilmer, F. Passmann, M. Gehl, G. Khitrova, and A.D. Bristow, *Phys. Rev. B* **91**, (2015).
- ⁴⁷ C.N. Borca, T.H. Zhang, X.Q. Li, and S.T. Cundiff, *Chem Phys Lett* **416**, 311 (2005).
- ⁴⁸ Y.Z. Hu, R. Binder, S.W. Koch, S.T. Cundiff, H. Wang, and D.G. Steel, *Phys Rev B* **49**, 14382 (1994).
- ⁴⁹ D. Webber, L. Hacquebard, X. Liu, M. Dobrowolska, J.K. Furdyna, and K.C. Hall, *Appl. Phys. Lett.* **107**, 142108 (2015).
- ⁵⁰ X. Dai, A.D. Bristow, D. Karauskaj, and S.T. Cundiff, *Phys. Rev. A* **82**, 052503 (2010).
- ⁵¹ L. Yang and S. Mukamel, *Phys. Rev. B* **77**, 075335 (2008).